Switchable orbital polarization and magnetization in strained LaCoO_{3} films

Er-Jia Guo, Ryan D. Desautels, David Keavney, Andreas Herklotz, T. Zac Ward, Michael R. Fitzsimmons, and Ho Nyung Lee

Phys. Rev. Materials **3**, 014407 — Published 15 January 2019

DOI: 10.1103/PhysRevMaterials.3.014407

Switchable orbital polarization and magnetization in strained $LaCoO_3$ films

*Er-Jia Guo,[1, 2, 3, *] Ryan D. Desautels,[1] David Keavney,[4] Andreas Herklotz,[1, 5] T. Zac Ward,[1] Michael R. Fitzsimmons,[1, 6] and Ho Nyung Lee [1, *]*

[1] *Oak Ridge National Laboratory, Oak Ridge, TN 37831, USA*
[2] *Beijing National Laboratory for Condensed Matter Physics, Institute of Physics, Chinese Academy of Sciences, Beijing 100190, China*
[3] *Center of Materials Science and Optoelectronics Engineering, University of Chinese Academy of Sciences, Beijing 100049, China*
[4] *Advanced Photon Source, Argonne National Laboratory, Argonne, Illinois 60439, USA*
[5] *Institute for Physics, Martin-Luther-University Halle-Wittenberg, Halle (Saale) 06120, Germany*
[6] *Department of Physics and Astronomy, University of Tennessee, Knoxville, TN 37996, USA*

Corresponding author: ejguo@iphy.ac.cn and hnlee@ornl.gov

Abstract

Strain engineering of epitaxial heterostructures offers opportunities to control the orbital degree of freedom by lifting the degeneracy of e_g states. Here, we show that the orbital occupation in $LaCoO_3$ (LCO) films can be switched between two degenerate e_g bands with epitaxial strain. The orbital polarization of nearly -100% (or 100%) is controlled by depleting occupation of $d_{x^2-y^2}$ (or $d_{3z^2-r^2}$) orbital entirely in LCO for large compressive (or moderate tensile) strain. The change of electronic configuration associated with the spin state transition modulates the magnetization of strained LCO films. Under compressive strain, LCO films exhibit a small magnetization without long-range ferromagnetic ordering. With tensile strain increases, the magnetization of the LCO films increases and reaches the maximum value when the bonding angle (Co-O-Co) is close to 180° and the in-plane bond length (Co-O) is unstretched. Our results highlight the role of octahedral distortion and spin state crossover in tailoring the magnetic properties of cobaltite thin films, suggesting an attractive route to deliberately control the orbital polarization that can be tuned to maximize the functionality of oxide heterostructures.

Keywords: Orbital polarization; ferromagnetism; strain engineering; X-ray scattering; ferroelastic materials

Complex oxide heterostructures have attracted considerable interest because many novel phenomena can be realized using dimensional confinement and strain manipulation. Lanthanum cobaltite, $LaCoO_3$ (LCO), is an example in this context. The low-temperature magnetic susceptibility of bulk LCO was found to have three contributions: a Curie-Weiss paramagnetism, a thermally driven spin-state transition, and a surface-related ferromagnetism with $T_c \approx 85$K. It was found that the spin state configuration of Co^{3+} ions transits from a low spin (LS, t_{2g}^6, $S = 0$) state to an intermediate- (IS, $t_{2g}^5 e_g^1$, $S = 1$) or a high-spin state (HS, $t_{2g}^4 e_g^2$, $S = 2$) with increasing temperature. [1-4] Previous work with strained thin films reported that LCO thin films under tensile strain exhibited ferromagnetism at low temperatures. [5-11] To date, the exact origin of the ferromagnetism in LCO films is still controversial. Multiple competing mechanisms have been proposed to explain the enhancement of magnetization, including spin state transition, [5-7] orbital ordering, [8] and defect (oxygen vacancy) formation. [9-11] The first scenario is supported by both experiment and theoretical calculation in which epitaxial strain plays a critical role in the spin state transition. [7, 12] In this scenario, a small change of strain in LCO films could influence both crystal field splitting (Δ_{cf}) and intra-atomic exchange interaction (Δ_{ex}) through octahedral distortions. [5-7, 13, 14] The balance between Δ_{cf} and Δ_{ex} directly governs the spin states of Co ions, giving rise to the observed ferromagnetism in the strained LCO films. To test this hypothesis, a systematic study of strain effects on the electronic and magnetic properties is required.

Previously, both static [6, 7] and reversible-controlled strain effects [15] on the magnetization of LCO films have been investigated. It is generally believed that tensile strain in the LCO films increases the population of higher spin state Co^{3+} ions, *i.e.* the intermediate spin (IS, $t_{2g}^5 e_g^1$) and high spin (HS, $t_{2g}^4 e_g^2$) configurations, resulting in an enhanced magnetization. [5-7] Previous work, [6, 7] addressed these issues in films with a relatively narrow strain window (~

3.5%), and at thicknesses (above 50 nm) which allowed partial relaxation in LCO films. To understand the connection between the electronic state and magnetization, it is necessary to systematically cover a range of lattice symmetries to map the structure-function response where relaxation does not complicate the interpretation of the observed physical responses. Using soft x-ray absorption spectroscopy (XAS), we investigated the electronic and magnetic properties of coherently strained epitaxial LCO thin films varying strain over a wide range. We show that the orbital polarization in LCO films is strongly modulated by epitaxial strain, suggesting the key role of strain-mediated spin state transition in the competing spin-orbital entanglement.

High-quality LCO thin films were epitaxially grown on a set of single crystalline substrates, including $SrLaAlO_4$ (SLAO), $LaAlO_3$ (LAO), $NdGaO_3$ (NGO), $(LaAlO_3)_{0.3}$-$(SrAl_{0.5}Ta_{0.5}O_3)_{0.7}$ (LSAT), $SrTiO_3$ (STO), $DyScO_3$ (DSO), and $GdScO_3$ (GSO) (Figure 1a), using pulsed laser deposition. Samples were grown at 700 ^{o}C in oxygen partial pressure of 100 mTorr. The thickness of LCO layer was 40 unit cells (u. c.) (approximately 14 nm). Subsequently, a 5 u. c.-thick STO capping layer was grown on each LCO layer to prevent the loss of oxygen at the surface. [7] The samples were cooled at a rate of 5 ^{o}C/min to room temperature in oxygen partial pressure of 100 Torr. X-ray reflectivity measurements were conducted to confirm the layer thicknesses in design and the abrupt interfaces between the films and substrates. We performed X-ray diffraction (XRD) measurements on all samples (see Fig. S1 in Ref [16]). XRD θ–2θ scans around the 002 reflection of LCO films grown on various substrates showed distinct thickness fringes around Bragg peaks (Figure 1b), exhibiting a good crystalline quality for all LCO films. XRD reciprocal space maps (RSMs) indicate that all LCO films are coherently strained to the substrates with negligible strain relaxation (Figure 1c). The in-plane misfit strain (ε_{xx}) of the LCO films varies from –1.4% (compressive) to 4.1% (tensile)

depending upon the substrate. The out-of-plane lattice parameters of the LCO films are also obtained from the RSMs. The out-of-plane strain (ε_{zz}) of the LCO films spans a range from 2.2 to -2.3%. We calculated $\Delta\varepsilon_{xx}/\Delta\varepsilon_{zz}$ to be −0.82, yielding a Poisson ratio of LCO $v = 1/(1 - 2 \times \Delta\varepsilon_{xx}/\Delta\varepsilon_{zz}) \approx 0.38$, which is close to the literature value of 0.33. [17, 18] This result suggests that the substrate-induced misfit strain is accommodated by the elastic deformation of the LCO films.

We first discuss the influence of strain on the electronic properties of the LCO films using element-specific X-ray absorption spectroscopy (XAS). The XAS was collected around the O *K*-edge and Co *L*-edge in total florescence yield (FY) mode. Figure 2a shows XAS at O *K*-edge for LCO films grown on various substrates. For all of the LCO films (except for the LCO/DSO sample), we observed distinct pre-peaks at around 530 eV, corresponding to the excitation from the O 1*s* state to the hybridized O 2*p*-Co^{3+} 3*d* state. [18] These pre-peaks overlapped with the characteristic peaks from different substrates, hindering the quantitatively analysis of the hybridization strength between the Co and O (Figure 2a, and Fig. S2 in Ref. [16]). Direct comparison of XAS data from LCO films with reference spectra of Co^{2+} [19] and Co^{3+} ions [20] indicates no detectable Co^{2+} for the capped LCO films (see Fig. S3 in Ref. [16]). Using Gaussian fitting to the XAS for Co L_3-edge, we estimate an upper limit of 2 % for the content of Co^{2+}. The shoulders at ~ 782 eV (for Co L_3-edge) and at ~ 797 eV (for Co L_2-edge) are the fingerprints for the LS state Co^{3+} present in the LCO films. [21]

The electronic configuration of the LCO films was further characterized by X-ray linear dichroism (XLD) using out-of-plane (I_{oop}) and in-plane (I_{ip}) linearly polarized X-ray beams (Figure 2b). One can anticipate that the absorption of X-rays polarized along $E_{oop}//c$ (or $E_{ip}//ab$) arises largely from the unoccupied Co $d_{3z^2-r^2}$ (or $d_{x^2-y^2}$) orbitals, *i. e.* the holes. [19, 20] The difference between I_{oop} and I_{ip} directly reflects the orbital configuration of *d* electrons (Figure 3a).

For the unstrained bulk LCO, a degenerated orbital occupancy is expected, thus no XLD signal is observed. For LCO films under compressive strain, the position of energy peak in I_{oop} is lower than that of I_{ip}. This result indicates that the electrons preferentially occupy the $d_{3z^2-r^2}$ orbital rather than the $d_{x^2-y^2}$ orbital (Figure 3b). Thus, the XLD peaks show positive values for the compressive-strained LCO films. However, for tensile-strained LCO films, the peaks around the Co *L*-edge exhibited negative values, suggesting a higher electron occupancy in the $d_{x^2-y^2}$ orbital compared to the $d_{3z^2-r^2}$ orbital (Figure 3b). The orbital occupancy strongly depends on the strain states of LCO films. The orbital polarization (*P*) can be quantitatively determined using X-ray dichroism sum rules. [22] $P = (n_{x^2-y^2} - n_{3z^2-r^2})/(n_{x^2-y^2} + n_{3z^2-r^2})$, where $n_{x^2-y^2}$ and $n_{3z^2-r^2}$ represent the number of electrons. *P* abruptly changes its sign when the strain state of LCO films changes from compressive to tensile strain (Figure 3c). We find that *P* is close to -100% and 100% for the LCO films grown on SLAO and LSAT substrates, respectively. These results suggest the electron occupation in these two cases can be modulated from a nearly empty to a fully occupied $d_{x^2-y^2}$ orbital by changing the misfit strain. As the tensile strain further increases above 1.6%, *P* reduces again towards zero, indicating that the electrons tend to be equally distributed over the $d_{x^2-y^2}$ and $d_{3z^2-r^2}$ orbitals for tensile strain beyond 3 %.

The strain modulated electronic state is accompanied by a change in the magnetic ground state of the LCO films. Macroscopic magnetic measurements were performed on the LCO films grown on various diamagnetic substrates, as shown in Figure 1d and 1e. Our measurements show a minimal magnetic response for the compressive-strained LCO films (on SLAO and LAO). In contrast, ferromagnetic hysteresis loops were observed for tensile-strained LCO films. We note that the *M*(*H*) does not saturate above 1 T, but continuously increase as increasing the magnetic

field. The saturated magnetization is ~ 2.1 μ_B/Co and ~ 1.3 μ_B/Co for LCO films grown on LSAT and STO substrates, respectively. These results suggest that an additional paramagnetic (PM) component in the LCO films contributes to the total magnetization. [2, 5-7] Meanwhile, we found that a small change of strain strongly affects the magnetization of LCO films, whereas no significant changes were observed for the Curie temperature (T_c ~ 80 K). These observations are consistent with previous reports. [5-10]

To eliminate the influence of paramagnetism from the substrates on the magnetometry data, we compare the X-ray magnetic circular dichroism (XMCD) at Co *L*-edge for all LCO films which cover a wide range of misfit strain. The XMCD measurements were performed at 10 K under a field of ± 5 T applied along the in-plane direction. XMCD signals were observed for all samples (Figure 4a). The signals at the Co L_2- and L_3-edges have opposite signs. We confirm that the XMCD signals flip sign with the reversal of the applied magnetic fields (± 5 T), thus the XMCD exhibits magnetic response under the applied fields. The intensity of the XMCD signal varies with the strain state of the LCO film. The magnetization of LCO films is quantitatively estimated using spin sum rules to separate the orbital (*L*) and spin (*S*) contributions to the total magnetization ($M = L + 2S$). [23] Total magnetization of LCO films is dominated by the spin contribution (Figure 4b), which is typical for 3*d* transition metal oxides with relatively low spin-orbital coupling. For the moderately tensile-strained LCO film on LSAT, the *S* and *L* reach maximum and minimum values, respectively, resulting in the largest *M* among all LCO films. Figure 4b compares the total magnetization of strained LCO films derived from the XMCD signal (solid circles) and direct measurements from SQUID magnetometry (triangles). The results from both techniques are consistent.

The intriguing strain dependence on the electronic and magnetic properties of the LCO films arise from the structural distortion induced spin state transition in Co ions. In bulk LCO ($R\bar{3}c$, rhombohedral lattice structure), the Co-O bond length (d) is 1.93 Å and the Co-O-Co bonding angle (β) ≈ 163°. [24- 26] The spin state of Co ions is determined by the electronic configuration of the t_{2g} and e_g bands. The transition between different spin states is controlled by the energy difference (ΔE) between the crystal field splitting energy (Δ_{cf}) and the intra-atomic exchange interaction energy (Δ_{ex}). In addition, the distortion of CoO_6 octahedra in the strained LCO films will further split the e_g band into $d_{x^2-y^2}$ and $d_{3z^2-r^2}$ orbitals. Thus, another factor, the bandwidth (W) of the hybridized Co e_g orbital and O p orbital, contributes to the energy difference $\Delta E = \Delta_{cf} - \Delta_{ex} - W/2,$ where $\Delta_{cf} \propto 1/d^5$ and $W \propto \cos(\pi - \beta)/d^{3.5}$. [3, 27] Under compressive strain, the CoO_6 octahedra distort by shrinking β and decreasing d to accommodate the in-plane compression. [28] In this case, ΔE will be larger for the compressive strain compared to the tensile strain. Thus, the Co e_g bands will primarily empty the higher energetic $d_{x^2-y^2}$ orbital, resulting in a large negative orbital polarization (Figure 3c) and a comparatively lower spin states, *e.g.*, a mixture of LS and IS. The spin state yields a small magnetization observed in compressive-strained LCO films. As the strength of compressive strain reduces, the distorted lattices increase β towards 180° while keeping d unchanged. Thus, the bandwidth is broadened, and the crystal field energy reduces, leading to a decreased ΔE. In this situation, the higher spin state becomes more energetically favorable. This favors the HS and IS states and reduces the population of LS state as the tensile strain increases. The magnetization of LCO films will continuously increase as the strain state of LCO films changes from compressive to moderate-tensile strain.

For LCO films coherently strained on LSAT, the in-plane lattice constant of LCO films ($a_{LCO} = a_{LSAT} = 3.86$ Å) is approximately twice the Co-O bond length in bulk LCO ($d = 1.93$ Å). In this case, d is not stretched, and β would remain 180°. The bandwidth reaches its maximum value $1/d^{3.5}$, suggesting the strongest hybridization between the Co 3d and O 2p orbitals (qualitative comparisons in Figure 2a). In this case, the Co^{3+} spin state favor HS with relatively small contribution from IS and LS states. According to the Goodenough-Kanamori-Anderson (GKA) rules, [29, 30] this spin configuration favors ferromagnetic superexchange between the occupied and unoccupied e_g orbitals. Therefore, the LCO films grown on LSAT exhibit the largest magnetization. Further increase of tensile strain in LCO films (*e. g.*, on STO, DSO, and GSO) will not increase the bonding angle as β = 180°; instead, d stretches along the in-plane direction, resulting in a continuous decrease of $(\Delta_{cf} - W/2) \approx (1/d^5 - 1/d^{3.5})$. Then, ΔE further decreases. The large reduction in ΔE might leads to the strong overlap between the t_{2g} and e_g bands, depopulating the $d_{x^2-y^2}$ orbital in favor of the t_{2g} band. This hypothesis is supported by our observations of both reduced orbital polarization (Figure 3c) and magnetization (Figure 4b). This result ultimately suggests that Co^{3+} ions transit from a higher spin state to a lower one with tensile strain beyond 1.6%.

Octahedral tilting and rotations in the LCO thin films may play a role in the modification of the magnetic properties. [31-33] The symmetry of the substrates used in the present study varies from rhombohedral (LAO), cubic (SLAO, LSAT, and STO), to orthorhombic (NGO, DSO, and GSO) lattice structures with varying octahedral rotation patterns. It is challenging to draw a complete picture of the influence of substrate-induced octahedral rotation on the overall magnetic response of our LCO films. Earlier work has shown that a modification of octahedral tilt / rotation commonly exists at oxide interfaces within a few unit cells. [34-36] So, a small

portion of the thin film's magnetization may be affected. Nevertheless, the magnetization derived from XMCD and magnetometry is dominated by the film bulk, where epitaxial strain plays a major role. Further work involving depth dependent magnetization and microscopic structural profiles is required to ascertain whether a correlation between octahedral tilt and rotation and the interfacial magnetization in the LCO films.

In summary, strain effects on the electronic and magnetic properties of epitaxial LCO thin films were investigated using XAS and magnetometry. We found that the orbital occupation can be effectively switched between the two degenerate e_g orbitals (as evidenced by change of orbital polarization) by epitaxial strain. The magnetic properties of the LCO films were strongly associated with the electronic state of the Co ions, which was controlled by the interplay among the crystal field splitting, orbital bandwidth, and inter-atomic exchange interaction. The higher spin states are not only stabilized by a decrease of the crystal field energy, but also by an increase of bandwidth, *i.e.,* the bonding angle and bond length. The largest magnetization was observed in a LCO film on LSAT under a moderate-tensile strain state, in which the bonding angle is close to 180^o and the bond length is not stretched above the bulk value. Further stretching the film along the in-plane direction reduced the magnetization of LCO films. Our work suggests a powerful route to tailor physical properties through strain tuning that effectively manipulates the orbital occupancy of cobalt ions.

Acknowledgements

We thank Yaohua Liu, Changhee Sohn, and Hyoungjeen Jeen for valuable discussions. This work was supported by the U.S. Department of Energy (DOE), Office of Science, Basic Energy Sciences, Materials Sciences and Engineering Division. T. Z. W. was supported through the DOE Early Career Research Program for a part of magnetic data analysis. This research used

resources of the Advanced Photon Source, a U.S. DOE Office of Science User Facility operated by Argonne National Laboratory under Contract No. DE-AC02-06CH1135 (XAS). This work was partly supported by the Hundred Talent Program from Chinese Academy of Sciences during manuscript revision and further data analysis.

References

[1] V. K. Wadhawan, *Ferroelasticity and related properties of crystals*, Phase Transitions **3**, 3-103, (1982).

[2] J.-Q. Yan, J.-S. Zhou, and J. B. Goodenough, *Ferromagnetism in $LaCoO_3$*, Phys. Rev. B **70**, 014402 (2004).

[3] J. –S. Zhou, J. –Q. Yan, and J. B. Goodenough, *Bulk modulus anomaly in $RCoO_3$ (R=La, Pr, and Nd)*, Phys. Rev. B **71**, 220103(R) (2005).

[4] P. E. Vullum, R. Holmestad, H. L. Lein, J. Mastin, M. - A. Einarsrud, and T. Grande, *Monoclinic Ferroelastic Domains in $LaCoO_3$ - Based Perovskites*, Adv. Mater. **19**, 4399-4403 (2007).

[5] D. Fuchs, C. Pinta, T. Schwarz, P. Schweiss, P. Nagek, S. Schuppler, R. Scheider, M. Merz, G. Roth, and H. v. Löhneysen, *Ferromagnetic order in epitaxially strained $LaCoO_3$ thin films*, Phys. Rev. B **75**, 144402 (2007).

[6] D. Fuchs, E. Arac, C. Pinta, S. Schuppler, R. Schneider, and H. v. Löhneysen, *Tuning the magnetic properties of $LaCoO_3$ thin films by epitaxial strain*, Phys. Rev. B **77**, 014434 (2008).

[7] W. S. Choi, J. –H. Kwon, H. Jeen, J. E. Hamann-Borrero, A. Radi, S. Macke, R. Sutarto, F. He, G. A. Sawatzky, V. Hinkov, M. Kim, and H. N. Lee, *Strain-Induced Spin States in Atomically Ordered Cobaltites*, Nano Lett., **12**, 4966–4970 (2012).

[8] J. Fujioka, Y. Yamasaki, H. Nakao, R. Kumai, Y. Murakami, M. Nakamura, M. Kawasaki, and Y. Tokura, *Spin-Orbital Superstructure in Strained Ferrimagnetic Perovskite Cobalt Oxide*, Phys. Rev. Lett. **111**, 027206 (2013).

[9] N. Biškup, J. Salafranca, V. Mehta, M. P. Oxley, Y. Suzuki, S. J. Pennycook, S. T. Pantelides, and M. Varela, *Insulating Ferromagnetic $LaCoO_{3-\delta}$ Films: A Phase Induced by Ordering of Oxygen Vacancies*, Phys. Rev. Lett. **112**, 087202 (2014).

[10] V. V. Mehta, N. Biskup, C. Jenkins, E. Arenholz, M. Varela, and Y. Suzuki, *Long-range ferromagnetic order in $LaCoO_{3-\delta}$ epitaxial films due to the interplay of epitaxial strain and oxygen vacancy ordering*, *Phys. Rev. B* **91**, 144418 (2015).

[11] J. H. Jang, Y. –M. Kim, Q. He, R. Mishra, L. Qiao, M. D. Biegalski, A. R. Lupini, S. T. Pantelides, S. J. Pennycook, S. V. Kalinin, and A. Y. Borisevich, *In Situ Observation of Oxygen Vacancy Dynamics and Ordering in the Epitaxial $LaCoO_3$ System*, *ACS Nano*, **11** (7), 6942–6949 (2017).

[12] J. –H. Kwon, W. S. Choi, Y. –K. Kwon, R. Jung, J. –M. Zuo, H. N. Lee, and J. Kim, *Nanoscale Spin-State Ordering in $LaCoO_3$ Epitaxial Thin Films*, *Chem. Mater.*, **26**, 2496−2501 (2014).

[13] G. E. Sterbinsky, R. Nanguneri, J. X. Ma, J. Shi, E. Karapetrova, J. C. Woicik, H. Park, J.-W. Kim, and P. J. Ryan, *Ferromagnetism and Charge Order from a Frozen Electron Configuration in Strained Epitaxial $LaCoO_3$*, Phys. Rev. Lett. **120**, 197201 (2018).

[14] Y. Yokoyama, Y. Yamasaki, M. Taguchi, Y. Hirata, K. Takubo, J. Miyawaki, Y. Harada, D. Asakura, J. Fujioka, M. Nakamura, H. Daimon, M. Kawasaki, Y. Tokura, and H. Wadati, *Tensile-Strain-Dependent Spin States in Epitaxial $LaCoO_3$ Thin Films*, Phys. Rev. Lett. **120**, 206402 (2018).

[15] A. Herklotz, A. D. Rata, L. Schultz, and K. Dörr, *Reversible strain effect on the magnetization of $LaCoO_3$ films*, Phys. Rev. B **79**, 092409 (2009).

[16] See Supplemental Material at http://link.aps.org/supplemental/**** for details of full-range (0-120°) XRD patterns of strained LCO films, the XAS O *K*-edge data for strained LCO films and underlying substrates, and the XAS Co L-edge data for LCO films with/ without STO ultrathin capping layer.

[17] N. Orlovskaya, K. Kleveland, T. Grande, and M. A. Einarsrud, *Mechanical Properties of $LaCoO_3$-Based Ceramics*, J. Eur. Ceram. Soc. **20**, 51-56 (2000).

[18] M. Lugovy, A. Aman, Y. Chen, N. Orlovskaya, J. Kuebler, T. Graule, M. J. Reece, D. Ma, A. D. Stoica, and K. An, *In-situ neutron diffraction of $LaCoO_3$ perovskite under uniaxial compression. II. Elastic properties*, *J. Appl. Phys.* **116**, 013504 (2014).

[19] N. P. Lu, P. Zhang, Q. Zhang, R. Qiao, Q. He, H. –B. Li, Y. J. Wang, J. W. Guo, D. Zhang, Z. Duan, Z. L. Li, M. Wang, S. Z. Yang, M. Z. Yan, E. Arenholz, S. Y. Zhou, W. L. Yang, L. Gu, C. W. Nan, J. Wu, Y. Tokura, P. Yu, *Electric-field control of tri-state phase transformation with a selective dual-ion switch*, Nature **546**, 124 (2017).

[20] M. W. Haverkort, Z. Hu, J. C. Cezar, T. Burnus, H. Hartmann, M. Reuther, C. Zobel, T. Lorenz, A. Tanaka, N. B. Brookes, H. H. Hsieh, H.-J. Lin, C. T. Chen, and L. H. Tjeng, *Spin State Transition in $LaCoO_3$ Studied Using Soft X-ray Absorption Spectroscopy and Magnetic Circular Dichroism*, Phys. Rev. Lett. **97**, 176405 (2006).

[21] Z. Hu, H. Wu, M. W. Haverkort, H. H. Hsieh, H. J. Lin, T. Lorenz, J. Baier, A. Reichl, I. Bonn, C. Felser, A. Tanaka, C. T. Chen, and L. H. Tjeng, *Different Look at the Spin State of Co^{3+} Ions in a CoO_5 Pyramidal Coordination*, Phys. Rev. Lett. **92**, 207402 (2004).

[22] G. van der Laan, *Sum rules and fundamental spectra of magnetic X-ray dichroism in crystal field symmetry*, J. Phys. Soc. Jpn. **63**, 2393–2400 (1994).

[23] G. Schütz, W. Wagner, W. Wilhelm, P. Kienle, R. Zeller, R. Frahm, and G. Materlik, *Absorption of circularly polarized x rays in iron*, Phys. Rev. Lett. **58**, 737 (1987).

[24] K. Gupta and P. Mahadevan, *Strain-driven magnetism in $LaCoO_3$ thin films*, Phys. Rev. B **79**, 020406(R) (2009).

[25] P. G. Radaelli and S. W. Cheong, *Structural phenomena associated with the spin-state transition in $LaCoO_3$*, Phys. Rev. B 66, 094408 (2002).

[26] I. A. Nekrasov, S. V. Streltsov, M. A. Korotin, and V. I. Anisimov, *Influence of rare-earch ion radii on the low-spin to intermediate-spin state transition in lanthanide cobaltite perovskites: $LaCoO_3$ versus $HoCoO_3$*, Phys. Rev. B **68**, 235113 (2003).

[27] W. A. Harrison, *The Electronic Structure and Properties of Solids* (Freeman, San Francisco, 1980).

[28] T. Vogt, J. A. Hriljac, N. C. Hyatt, and P. Woodward, *Pressure-induced intermediate-to-low spin state transition in $LaCoO_3$*, Phys. Rev. B **67**, 140401(R) (2003).

[29] J. B. Goodenough, *Magnetism and the Chemical Bond* (Interscience-Wiley, New York, 1963).

[30] P. M. Raccah, and J. B. Goodenough, *First-order localized-electron versus collective-electron transition in $LaCoO_3$*, Phys. Rev. **155**, 932 (1967).

[31] J. M. Rondinelli, and N. A. Spaldin, *Structure and properties of functional oxide thin films: insights from electronic-structure calculations.* Adv. Mater. **23**, 3363–3381 (2011).

[32] E. J. Moon, P. V. Balachandran, B. J. Kirby, D. J. Keavney, R. J. Sichel-Tissot, C. M. Schlepütz, E. Karapetrova, X. M. Cheng, J. M. Rondinelli, and S. J. May, *Effect of Interfacial Octahedral Behavior in Ultrathin Manganite Films*, Nano Lett., **14** (5), 2509–2514, (2014).

[33] A. J. Grutter, A. Vailionis, J. A. Borchers, B. J. Kirby, C. L. Flint, C. He, E. Arenholz, and Y. Suzuki, *Interfacial Symmetry Control of Emergent Ferromagnetism at the Nanoscale*, Nano Lett., **16** (9), 5647–5651 (2016).

[34] Z. Liao, M. Huijben, Z. Zhong, N. Gauquelin, S. Macke, R. J. Green, S. Van Aert, J. Verbeeck, G. Van Tendeloo, K. Held, G. A. Sawatzky, G. Koster, and G. Rijnders, *Controlled lateral anisotropy in correlated manganite heterostructures by interface-engineered oxygen octahedral coupling*, Nat. Mater. **15**, 425 (2016).

[35] M. Huijben, L. W. Martin, Y.-H. Chu, M. B. Holcomb, P. Yu, G. Rijnders, D. H. A. Blank, and R. Ramesh, *Critical thickness and orbital ordering in ultrathin $La_{0.7}Sr_{0.3}MnO_3$ films*. Phys. Rev. B **78**, 094413 (2008).

[36] X. Zhai, L. Cheng, Y. Liu, Ch. M. Schlepütz, S. Dong, H. Li, X. Zhang, S. Chu, L. Zheng, J. Zhang, A. Zhao, H. Hong, A. Bhattacharya, J. N. Eckstein, and C. Zeng, *Correlating interfacial octahedral rotations with magnetism in $(LaMnO_{3+\delta})_N/(SrTiO_3)_N$ superlattices*, Nature Commun. **5**, 4283 (2014).

Figures and figure captions

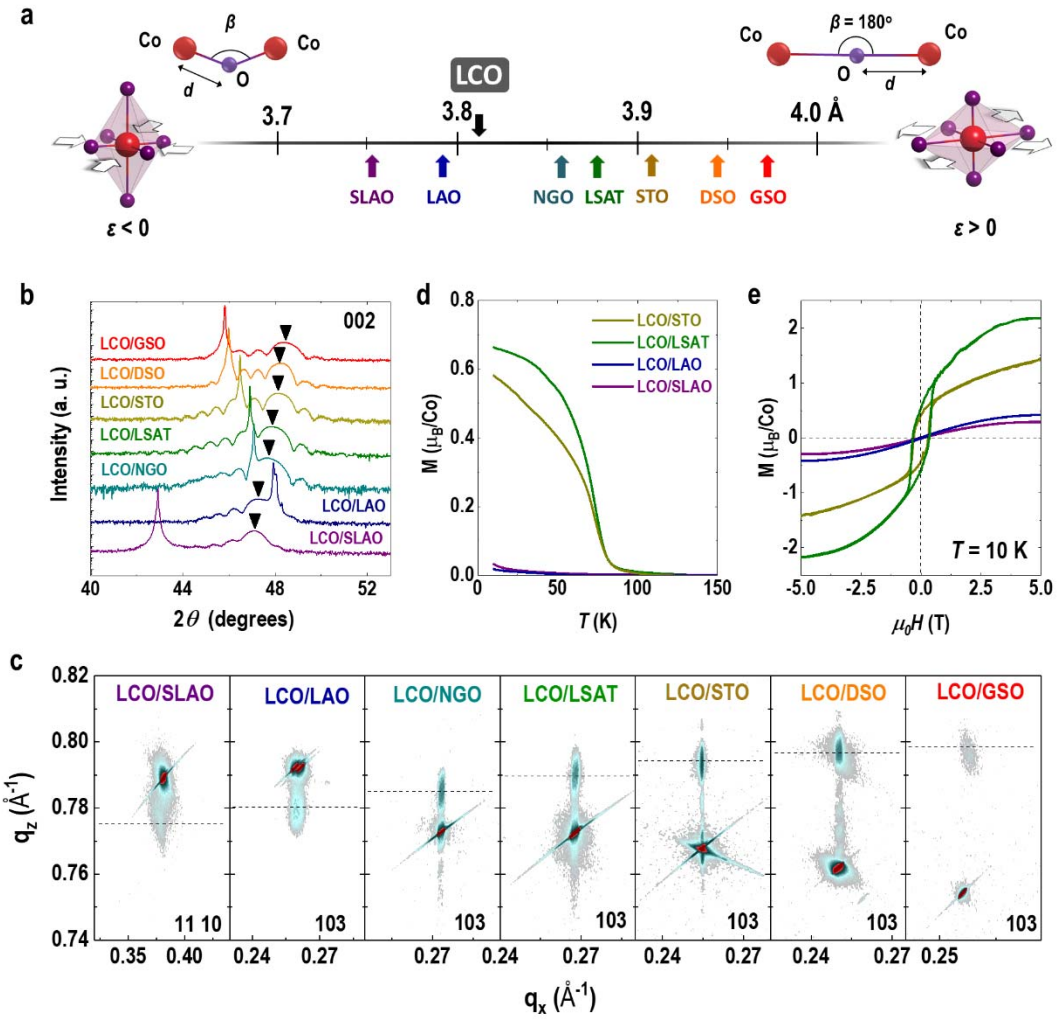

Figure 1 | **Structural properties of LCO films grown on various substrates. a**. Lattice parameters of the LCO bulk and various single crystal substrates [SLAO: $SrLaAlO_4$, LAO: $LaAlO_3$, NGO: $NdGaO_3$, LSAT: $(LaAlO_3)_{0.3}$-$(Sr_1Al_{0.5}Ta_{0.5}O_3)_{0.7}$, STO: $SrTiO_3$, DSO: $DyScO_3$, and GSO: $GdScO_3$]. Pseudocubic lattice constants were used for non-cubic substrates. Insets indicate the in-plane bond angle (Co-O-Co) β and the bond length (Co-O) d. **b**. XRD θ–2θ scans around the 002 reflection of LCO films grown on various substrates. The 002 peak of LCO films is indicated with "▼". The misfit strain of LCO films gradually changes from the compressive (SLAO, LAO) to the tensile strain (NGO, LSAT, STO, DSO, and GSO). **c**. Reciprocal space maps (RSMs) around substrate's 103 or 103_{pc} reflections (or the SLAO substrate's 1110 reflection). All films are coherently grown on the substrates. **d.** *M-T* curves and **e**. *M-H* hysteresis loops of LCO films grown on SLAO, LAO, STO, and LSAT substrates. The linear (or nonlinear) diamagnetic backgrounds from these substrates were subtracted. For the *M-T* curves, a magnetic field of 0.1 T was applied along the in-plane direction during the cooling and warm-up measurements. The magnetic hysteresis loops were measured at 10 K and the maximum magnetic fields of ± 5 T.

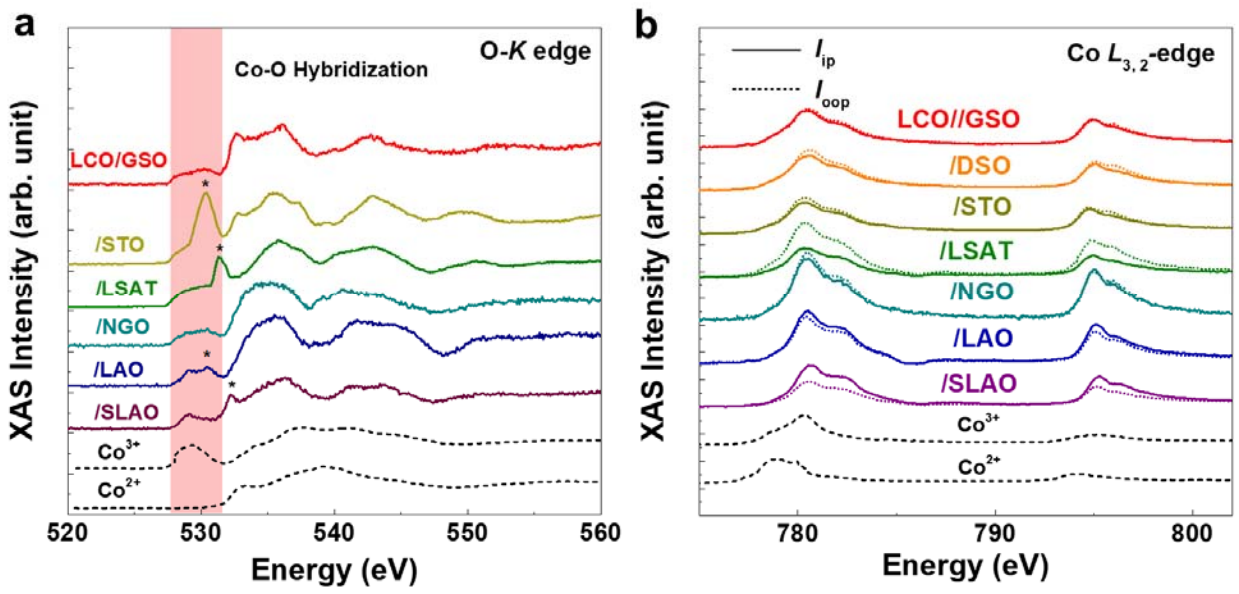

Figure 2 | X-ray absorption spectra (XAS) for LCO films grown on various substrates. a. XAS for O *K*-edge. The red-shaded region centered at ~530 eV represents the feature assigned to O 1*s* excitation to the Co 3*d*−O 2*p* hybridized state in LCO films. The asterisks (*) mark the O 1*s* excitation to the hybridized states between O 2*p* and other transition metals (for example, Ti, Ta, Al, Sr, *etc*.) from the substrates (detailed comparison in Fig. S2 in Ref. [16]). **b**. XAS for Co *L*-edges measured by the out-of-plane [I_{oop}, dashed lines, with the linear polarization vector, $E//c$] and in-plane [I_{ip}, solid lines, with $E//ab$] linearly polarized photons. All LCO films show strong peaks at around 780.5 eV and 795 eV, in consistent with the peak positions of the Co L_3- and L_2-edges for the Co^{3+} ions, respectively. XAS data confirm the valence state of the cobalt keeps 3+ independent of the LCO films' strain states. All spectra were collected and averaged over four times with fluorescence yield (FY) detection mode. The spectra from different samples are shifted for clarification. Dashed lines in both figures show the reference data from the Co^{2+} ions in $HSrCoO_{2.5}$ [19] and the Co^{3+} ions in LCO bulk. [20]

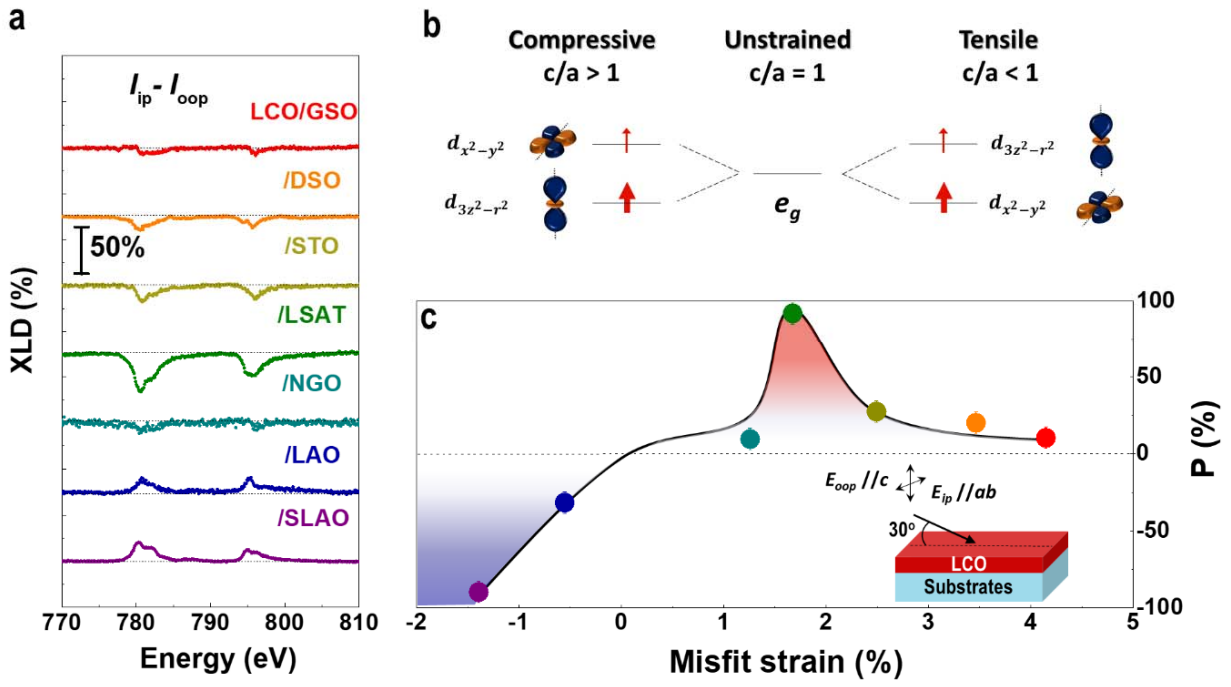

Figure 3 | Strain dependent electronic states of the LCO films. a. X-ray linear dichroism (XLD) of the LCO films grown on various substrates. XLD is calculated from the difference of X-ray absorption between in-plane (I_{ip}) and out-of-plane (I_{oop}) polarized photons. The spectra from different samples are shifted for clarification. The scale bar in **a** is for reference. **b**. Schematic electronic configurations of e_g band in the Co^{3+} ions. In bulk LCO (unstrained), the e_g band does not split. When the LCO films are compressive-strained, the energy of $d_{3z^2-r^2}$ band is lower, thus holes occupy the $d_{x^2-y^2}$ band; the opposite trend occurs when the LCO films are under tensile-strain. **c.** Misfit strain dependent orbital polarization P $[= (n_{x^2-y^2} - n_{3z^2-r^2})/(n_{x^2-y^2} + n_{3z^2-r^2})]$, where the $n_{x^2-y^2}$ and $n_{3z^2-r^2}$ represent the numbers of electrons. The largest P is observed for the LCO film grown on LSAT substrate. Inset of **d** shows the schematic of the X-ray scattering geometry for X-ray absorption spectroscopy (XAS) measurements. The incident angle of X-ray beam is ~ 30 degrees with respect to the sample's surface.

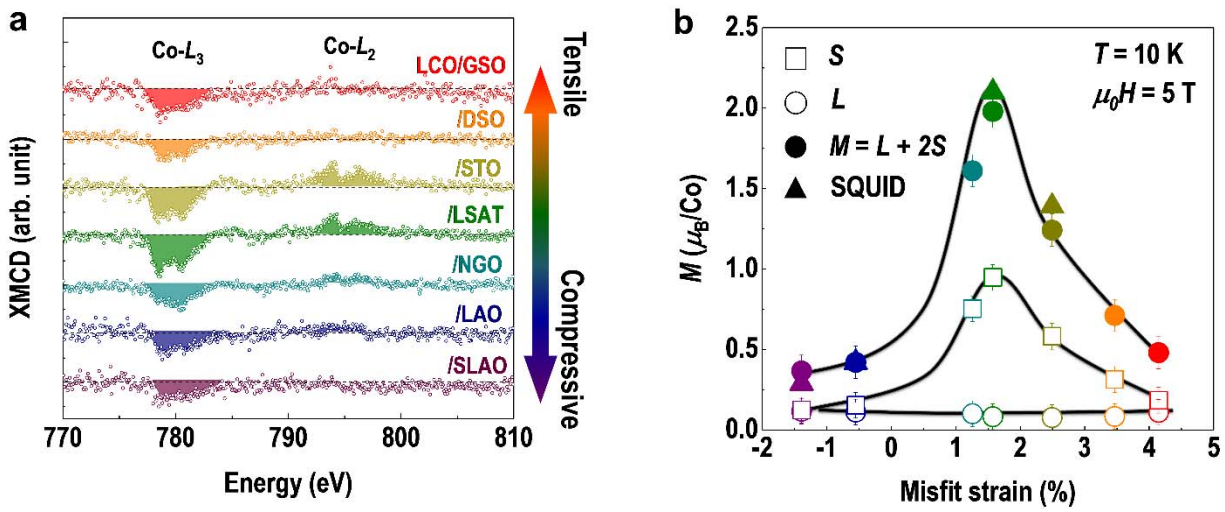

Figure 4 | Strain dependent magnetization of the LCO films. X-ray magnetic circular dichroism (XMCD) is imposed to systematically study the ferromagnetism of the LCO films under various strain states, as shown in **a**. The measurements are carried out at 10 K under an applied magnetic field of 5 T in bulk-depth probed fluorescence yield (FY) mode. The XMCD signals are calculated from the difference between μ^+ and μ^- divided by their sum, as described by $(\mu^+-\mu^-)/(\mu^++\mu^-)$, where μ^+ and μ^- denote XAS obtained from the right-hand circular polarized (RCP) and left-hand circular polarized (LCP) photons, respectively. The X-ray incident angle (30^o) and the circular polarization (96%) have been considered by multiplying $(\mu^+-\mu^-)/(\mu^++\mu^-)$ with [96%/cos(30^o)] ~ 1.1. The magnetization of the LCO films is quantitatively estimated using the spin sum rules to separate the orbital (L) and spin contribution (S) to the total magnetization ($M = L + 2S$). The calculated L, S, and M are summarized in **b**. We find the total magnetization derived from XMCD and SQUID (in **Figure 1e**) are consistent for the LCO films grown on SLAO, LAO, STO, and LSAT substrates.